Optical and dynamic nuclear polarization of ^{29}Si nuclei via photoexcited triplet states of oxygen-vacancy complexes in isotopically controlled silicon

T. Itahashi, H. Hayashi, M. R. Rahman, and K. M. Itoh*
School of Fundamental Science and Technology, Keio University, Yokohama 223-8522, Japan

L. S. Vlasenko, M. P. Vlasenko, and D. S. Poloskin
A. F. Ioffe Physico-Technical Institute, 194021, St. Petersburg, Russia
(Received 24 November 2012; published 6 February 2013)

Optical and dynamic nuclear polarization of ^{29}Si nuclei under saturation of the electron paramagnetic resonance (EPR) transitions of the photoexcited spin $S = 1$ states (Si-SL1 centers) of the oxygen + vacancy complexes (A-centers) have been investigated using silicon single crystals with various ^{29}Si nuclear abundances. The optical nuclear polarization alone led to the ^{29}Si nuclear polarization enhancement by a factor of ∼500 in the magnetic fields below 50 mT, and such enhancement was found to decrease significantly in the stronger fields up to 300 mT. On the other hand, saturation of the EPR lines of Si-SL1 centers having the electron spin polarization of 70–80% was transferred successfully to surrounding ^{29}Si nuclear spins to achieve the overall ^{29}Si nuclear spin polarization of ∼6.4%, and a method to increase up to 13–15% is proposed. The optimum condition to achieve such a high degree of nuclear polarization was found by systematic investigations of the dynamic nuclear polarization mechanisms.

DOI: 10.1103/PhysRevB.87.075201 PACS number(s): 76.70.Fz, 76.30.−v, 28.60.+s, 61.82.Fk

I. INTRODUCTION

Highly developed silicon technology, especially the fabrication of isotopically controlled bulk and layered silicon single crystals,[1–6] is expected to open the next stage for silicon-based quantum information processing devices.[7–15] Many of these applications employ electron and/or nuclear spins as qubits and require high spin polarization, i.e., initialization, at the start of quantum information processing and long coherence times for successful completion of the quantum algorithms. While the isotopic purification of host silicon matrix to eliminate background ^{29}Si stable isotopes of nuclear spin $I = 1/2$ is proven essential for achieving the large polarization[15–19] and long coherence times of electron[20–23] and nuclear[19] spins of donors in silicon, there are schemes that take advantage of ^{29}Si nuclear spins as qubits,[24–26] and thanks especially to the recent experimental demonstration of coherent quantum information transfer into and out of ^{29}Si nuclear spins in silicon,[27] exploration of physics leading to the high ^{29}Si nuclear spin polarization becomes important to reach at least 5% for implementation of the efficient algorithmic cooling protocol.[28]

The first, forced polarization of ^{29}Si nuclei was demonstrated by Abragam *et al.* by microwave irradiation of a phosphorus-doped silicon single crystal.[29,30] Here, they achieved the polarization of 0.048%, which corresponded to the enhancement by a factor of 30 with respect to its thermal equilibrium value.[29] An optical nuclear polarization (ONP) approach started by Lampel in 1968[31] reached 0.03% in 1982[32] and 0.25% in 2005.[33] Electron paramagnetic resonance- (EPR-) induced dynamic nuclear polarization (DNP) with lightly phosphorus-doped (∼10^{15} cm^{-3}) silicon achieved ^{29}Si polarization of 1.45%,[34,35] and this was limited by the long relaxation time of electrons bound to phosphorus donors (∼3×10^3 s at 1.2 K).[36] In similar DNP studies using lithium-doped silicon, the ^{29}Si polarization was limited to 0.72% due to the inhomogeneous broadening of EPR absorptions of electrons bound to isolated lithium and lithium-forming complexes with oxygen.[37] DNP of ^{29}Si with silicon microparticles has reached 2%,[38] and heavily doped (∼10^{17} cm^{-3}) phosphorus silicon bulk single crystals has achieved an impressive 10.4%.[39] While the physics leading to very high ^{29}Si polarization in microparticles[38] and in heavily doped silicon[39] is very interesting, employment of lightly doped silicon single crystals are preferred strongly for quantum information processing in order to retain the coherence time as long as possible. The present work shows a systematic investigation of dynamic ^{29}Si nuclear polarization using electron spins bound to photoexcited oxygen-vacancy (O-V) spin-triplet (SL1) centers,[40,41] leading to the maximum ^{29}Si nuclear polarization of ∼6.4%. The concentration of SL1 is low, of the order of 10^{15} cm^{-3}, and they exist only during the optical irradiation for initialization. As soon as the illumination is terminated, they decay to spin-singlet centers and do not act as sources of decoherence of surrounding spins.

Early experimental and theoretical investigations of DNP in solids[42–45] have shown that the maximum DNP degrees that can be achieved by the Overhauser effect[42,43] and solid effect[43–45] is equal to the equilibrium electron Boltzmann polarization of paramagnetic spin $S = 1/2$ centers. The maximal DNP enhancement E, the ratio of DNP degree P_N to the equilibrium Boltzmann nuclear polarization P_{N0}, is given by $E_{\max} = P_N/P_{N0} = P_{e0}/P_{N0} = \gamma_e/\gamma_N = 3310$ for silicon, where $\gamma_e = 28$ MHz/mT and $\gamma_N = 8.46$ kHz/mT are the electron and ^{29}Si nuclear gyromagnetic ratios, respectively. To achieve the highest P_N, the DNP experiments should be performed at low temperatures and at high magnetic fields. However, as mentioned above, the DNP experiments performed with phosphorus-doped silicon have shown that the efficiency of DNP process is limited by the long electron

spin-lattice relaxation time of paramagnetic phosphorus donors at low temperatures.[34,35] The DNP enhancement $E \approx 2680$ corresponding to ^{29}Si nuclear polarization $P_N = 1.45\%$ was demonstrated by saturating the Zeeman-split electron spin levels of phosphorus donors at the magnetic field $B = 320$ mT and $T = 12$ K, but E was much smaller at lower T due to the long electron relaxation time and at higher T due to ionization of the phosphorus donors.[34,35]

The idea to use the triplet centers for nuclear polarization has been suggested and realized in the experiments on ONP of protons in molecular crystals without applying the resonance microwave field.[46] Later, experiments on DNP using the EPR saturation of the photoexcited triplet centers in molecular crystals were performed,[47,48] and a new method of proton DNP using electron spin-locking effect was suggested.[49]

The photoexcited triplet (spin $S = 1$) centers in silicon, such as photoexcited neutral O-V complexes (Si-SL1),[50] Al-V complexes,[51] Sn-V complexes,[52] P-V complexes,[53] carbon-related centers,[54,55] and divacancies,[56] show advantages for DNP over the traditional spin $S = 1/2$ paramagnetic centers. Such centers are characterized by nonequilibrium populations of magnetic sublevels with different electron spin projections $m_S = +1$, 0, and -1, resulting from the spin-selective transitions from one of the three triplet levels to the spin-singlet ground state, i.e., exceptionally high polarization of electron spins leading to efficient DNP of the surrounding ^{29}Si nuclear spins is expected. The electron spin-lattice relaxation times of triplet centers are not relevant for ONP and DNP processes because under steady-state illumination, such centers are regenerated continuously from the relaxed singlet to excited triplet states by photoexcitation. Among different EPR spectra of the spin-triplet defects in silicon, the photoexcited triplet states of the neutral O-V complexes (Si-SL1 EPR spectrum[50]) yield the strongest EPR intensity. The O-V complexes, referred to as A-centers before photoexcitation, can be formed by electron-beam irradiation,[57] γ-ray irradiation,[58] or ion implantation[59] to create excess vacancies in Czochralski-grown silicon crystals containing the oxygen concentration of more than 10^{18} cm^{-3}. The A-centers are transformed to spin-triplet SL1 centers by illumination of band-edge light or injection of electrons and holes using diode structures without illumination.[58] A recent transient experiment with pulsed light has shown that A-centers are transformed to SL1 immediately after the light illumination followed by two electron spins bound to each SL1, reaching almost 100% polarization between magnetic sublevels with the timescale of 0.1 ms in the favorable temperature and external magnetic field condition, and such highly polarized triplets decay to singlet ground states with the timescale of a few milliseconds.[60] Under the continuous illumination employed in the present study, such photoexcitation and decay cycles are expected to occur continuously, and a certain steady-state condition is established among the ensemble of O-V centers, leading to large DNP of the surrounding ^{29}Si nuclear spins.

Therefore, we perform systematic experimental studies on DNP induced by saturation of the EPR transitions of photoexcited Si-SL1 centers in ^{29}Si isotopically controlled irradiated silicon crystals. Contribution of the optical excitation to nuclear polarization in DNP experiments will be analyzed in detail. The effects of ^{29}Si isotopic abundance on the EPR spectra of triplet centers and on the DNP will be shown. A variety of DNP features observed under saturation of the hyperfine (hf) EPR lines coupled to surrounding ^{29}Si nuclear spins is presented. The increase of DNP degrees by simultaneous saturation of some EPR lines appearing in several different magnetic field directions with respect to the silicon crystallographic orientation is discussed.

II. EXPERIMENTAL

The experiments were performed with n- and p-type Czochralski-grown silicon crystals containing 0.59, 4.7, and 99.2% of ^{29}Si isotope. Si samples doped with phosphorus ($N(\mathrm{P}) \approx 10^{15}$ cm^{-3}) and containing 0.59 and 99.2% of the ^{29}Si isotopes were irradiated at room temperature by γ-rays from the ^{60}Co source with the dose of 8×10^{18} γ/cm^2. In addition, two samples of n-Si ($N(\mathrm{P}) \approx 5 \times 10^{16}$ cm^{-3}) and high-resistance ($\sim$1000 Ω·cm) p-type Si with the natural (4.7%) abundance of the ^{29}Si isotopes were irradiated by 1-MeV electrons with the dose of 10^{18} e/cm^2 at room temperature.

A JEOL JES-RE3X X-band EPR spectrometer was used for detection of the EPR signals and for DNP of ^{29}Si nuclei through the saturation of EPR transitions at different values of magnetic field B_{sat}. The experiments were performed at the temperatures between 3.8 and 100 K using an Oxford Instruments (ESR900) helium gas flow cryostat. To create the excited spin $S = 1$ states of A-centers, samples placed in a cylindrical TE_{011} mode cavity were illuminated with a $\lambda = 1047$-nm line from a 2W Nd:YLF laser or by white light from a 100-W halogen lamp.

DNP was induced by saturation of a particular EPR transition using the same EPR spectrometer with a maximum microwave power of 200 mW at a fixed microwave frequency of 9.05 GHz. The magnetic field modulation amplitude B_m, from 10^{-2} to 1 mT, and microwave power were optimized for each investigated sample. The time of EPR saturation t was varied from 10 min to 3 h.

After the EPR saturation, the sample was transferred from the EPR spectrometer to a CMX300 CP/MAS nuclear magnetic resonance (NMR) spectrometer. The transfer time was typically 2 min. The long ^{29}Si nuclear spin-lattice relaxation time $T_{1N} > 1$ h for all samples at room temperature allowed to separate the EPR saturation and NMR measurements in time and space without the loss of signal intensity. To prevent fast nuclear relaxation and loss of nuclear polarization in the Earth's magnetic field, the samples were transferred to the NMR spectrometer using a small permanent magnet.

The ^{29}Si NMR signal was detected at room temperature using Fourier-transformed free-induction decay after a $\pi/2$ pulse with a magnetic field of 7 T, corresponding to the ^{29}Si NMR frequency of 60 MHz. The pulse length and the acquisition delay time after the $\pi/2$ pulse were 9 μs and 35 μs, respectively. The nuclear polarization degree and enhancement E was determined by comparing the integrated areas of the DNP-enhanced NMR signal $\mathrm{A}_{\mathrm{DNP}}$ with the area of the equilibrium NMR signal A_{eq}, detected in the 99.2% ^{29}Si

sample after 10–24 h of magnetization in the magnetic field of 7 T at 300 K. We employed relations

$$E = \frac{A_{\mathrm{DNP}}}{A_{\mathrm{eq}}} \cdot \frac{T}{300[K]} \cdot \frac{7\,[T]}{B_{\mathrm{sat}}}, \tag{1}$$

and

$$P_N = E\,P_{N0} = E \tanh\left(\frac{h\gamma_N B}{2kT}\right), \tag{2}$$

where T and B are the temperature and the magnetic field used for saturation in the EPR spectrometer, respectively, h is Planck's constant, k is Boltzmann's constant, and γ_N is the ^{29}Si gyromagnetic ratio. The equilibrium nuclear polarization degree is $P_{N0} = 4.8 \times 10^{-4}$ at $B = 7$ T and $T = 300$ K.

The equilibrium NMR signals were strong in the 99.2% ^{29}Si sample, while they were weak for samples with ^{29}Si isotope $f_{29\mathrm{Si}} < 4.7\%$. Therefore, values of P_N and E for low ^{29}Si samples were obtained by using A_{eq} values with respect to the 99.2% Si sample, taking into account the difference in the isotopic content. We used the ratio of the integrated NMR signals $A_{\mathrm{DNP}}/A_{\mathrm{eq}}$ rather than signal amplitudes ratio because of the dependence of the NMR line shape and linewidth on the ^{29}Si isotope amount.[24,61]

An exponential increase of nuclear polarization with saturation time t was observed in all the investigated samples. The steady-state values of the DNP enhancement, E^{ss}, DNP degree, $P_{\mathrm{N}}^{\mathrm{ss}}$, and nuclear polarization time T_{1N}^{p}, were determined using the fitting the exponential growth of the DNP NMR signal with the time t. In the case of illumination with the 100-W incandescent halogen lamp, the nuclear polarization time T_{1N}^{p} was in the range of 90–180 min, whereas under laser illumination the time was shorter, about 50–80 min, depending of the samples. It is found that the DNP process and values of E^{ss} and P_N^{ss} are the same between the halogen and laser excitations. The only difference appears in the nuclear polarization time T_{1N}^{p}, where the laser excitation is much shorter than that with the halogen lamp. At low temperatures (3.1–20 K), the equilibrium NMR signals cannot be observed because of extremely long nuclear spin-lattice relaxation time without illumination.

III. RESULTS AND DISCUSSION

The efficiency of the ^{29}Si DNP using the photoexcited triplet centers depends on a number of conditions: the concentrations of spin-triplet centers and ^{29}Si isotopes, the electron spin polarization, lifetime, and spin-lattice relaxation time of the triplet centers. The ^{29}Si nuclear spin polarization induced around the Si-SL1 centers expands to the whole sample by nuclear spin diffusion. For DNP via phosphorus in silicon, the ^{29}Si nuclear spin diffusion is relatively fast even for <4.7% ^{29}Si crystals, and it is the rate of DNP around the paramagnetic centers that limits the overall DNP rate.[35] The additional obstacle associated with DNP via phosphorus donors is the existence of the diffusion barriers, whereas such barriers disappear around SL1 upon relaxation to the ground singlet state. Therefore, the purpose of this section is to show the important features that eventually lead to optimization of the DNP condition to achieve the high ^{29}Si nuclear polarization.

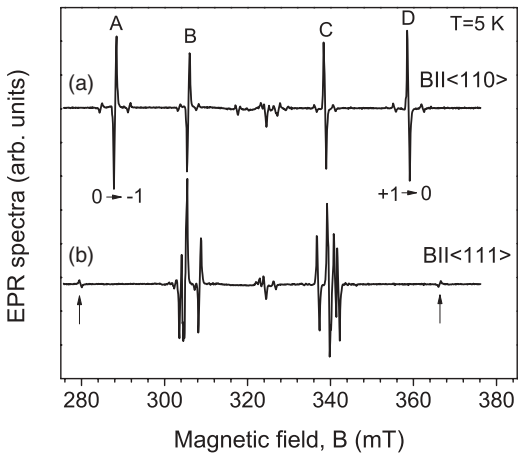

FIG. 1. EPR spectra detected under band-gap illumination in 1-MeV electron irradiated naturally and abounded (4.7% ^{29}Si) n-Si for $B \,||\, \langle 110\rangle$ (spectrum a) and $B \,||\, \langle 111\rangle$ (spectrum b). Weak lines at $B \approx 280$ and 366 mT (indicated by arrows in the spectrum b) correspond to the Si-PT1 EPR signals of the excited triplet states of $(\mathrm{C}_S\text{-}\mathrm{Si}_I\text{-}\mathrm{C}_S)^0$ centers (Refs. 54 and 65).

A. Photoexcited triplet states of oxygen + vacancy complexes in ^{29}Si isotope-controlled silicon

Without illumination, no EPR signal was observed in all the samples since the Fermi level is near the middle of forbidden gap and all radiation defects are not paramagnetic after the high dose of irradiation. Under or after the band-gap illumination, several overlapping weak EPR peaks of paramagnetic centers having spin $S = 1/2$ were observed. Such peaks included EPR of neutral phosphorus donors, negatively charged A-centers, and divacancies. An estimated total concentration of these light-induced paramagnetic centers was below 10^{15} cm^{-3}. A strong Si-SL1 signal emerged under steady-state illumination, as shown in Fig. 1. The lines labeled as A, B, C, D, and several weak lines at magnetic fields 320–330 mT originate from the excited triplet states of the neutral A-center.[50] The lines A and B of the Si-SL1 spectrum having the signs opposite to C and D correspond to emission of the microwave power, which shows that there is nonequilibrium distribution of populations between the $|+1\rangle$ and $|0\rangle$ and between $|0\rangle$ and $|-1\rangle$ states. In addition, the electron spin-lattice relaxation time T_{1S} is longer than the lifetime of the photoexcited triplet centers. The electron spin polarizations $P_e(+1,0)$ and $P_e(0,-1)$ between these sublevels are opposite

$$P_e(+1,0) = -P_e(0,-1) \gg P_{e0}, \tag{3}$$

where P_{e0} is the Boltzmann equilibrium polarization.

The spin Hamiltonian for spin $S = 1$ centers interacting with nuclear spin $\boldsymbol{I}$ in magnetic field $\mathbf{B}$ can be written as

$$H = \beta \mathbf{BgS} + \mathbf{SDS} + \mathbf{SAI} + \beta_N g_N \mathbf{BI}. \tag{4}$$

The first and last terms in Eq. (4) are electron and nuclear Zeeman energies, respectively, where $\beta\,(\beta_N)$ is the electron (nuclear) Bohr magneton, $\boldsymbol{g}$ is electron g-tensor, and g_N is nuclear g-factor. The second term describes dipole-dipole interactions between two electrons forming the total electron spin $S = 1$. The $\boldsymbol{D}$ tensor is the traceless tensor $(D_{xx} + D_{yy} + D_{zz} = 0)$, and two parameters $D = 3D_{zz}/2$ and

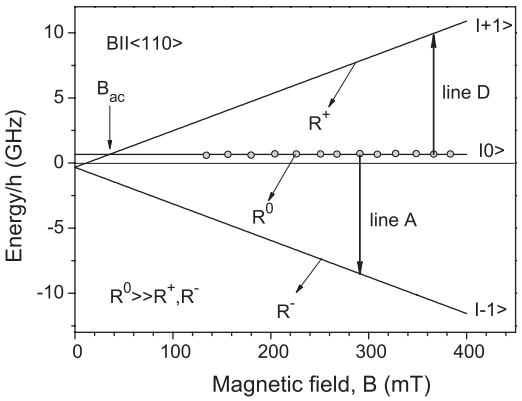

FIG. 2. Energy levels of the Si-SL1 center. Circles emphasize the overpopulation of the $|0\rangle$ level due to difference between probabilities R^+, R^0, and R^- of the transitions to the ground singlet state. B_{ac} corresponds to the anticrossing point of the $|+1\rangle$ and the $|0\rangle$ magnetic sublevels.

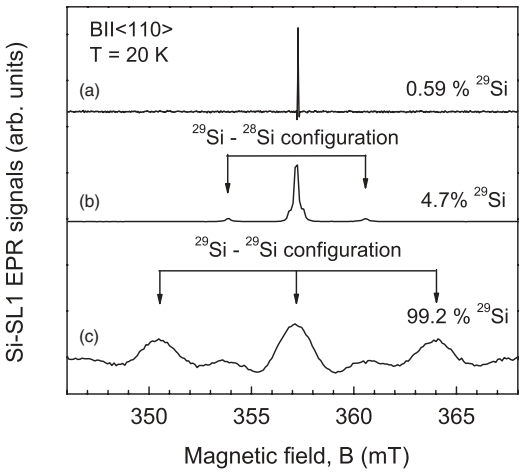

FIG. 3. The hf structure of the D line [see Fig. 1(a)] due to interactions between electrons and ^{29}Si nuclei occupying two nearest positions detected in irradiated silicon containing 4.7% (spectrum b) and 99.2% (spectrum c) ^{29}Si nuclei. In the sample with $f_{29\mathrm{Si}} = 0.59\%$ (a), the ^{29}Si hf satellites are too weak to be detected.

$E = (D_{xx} - D_{yy})/2$ are needed to describe the fine structure of the spin $S = 1$ EPR spectra. The third term in Eq. (4) corresponds to the hf interactions between electron and nuclear spins with the $\boldsymbol{A}$ tensor that includes both the isotropic contact and anisotropic dipole-dipole interactions.

The Si-SL1 spectrum exhibits the orthorhombic symmetry. The principal values of $\boldsymbol{g}$, $\boldsymbol{D}$, and $\boldsymbol{A}$ tensors were determined in Ref. 50. The maximum splitting $\Delta B \approx 70.3$ mT between the EPR lines [A and B in Fig. 1(a)] for $B \,||\, \langle 110\rangle$ corresponds to $D = 3D_{zz}/2 = -657.5 \times 10^{-4}$ cm^{-1} and anticrossing of magnetic sublevels with spin projections $m_S = +1$ and $m_S = 0$ is at $B_{ac} = \Delta B/2 \approx 35$ mT for $B \,||\, \langle 110\rangle$. As shown in Fig. 1(b), for $B \,||\, \langle 111\rangle$ all EPR lines are grouped near magnetic fields about 305 and 340 mT. The energy levels of the Si-SL1 center calculated for $B \,||\, \langle 110\rangle$ using spin Hamiltonian parameters determined in Ref. 50 are shown in Fig. 2.

The structure of the O-V center is well established; an oxygen atom localized near the substitution position forms chemical bonds with two neighbor Si atoms. The remaining two dangling bonds of silicon vacancy form the bonding and antibonding molecular orbitals oriented along any of six equivalent $\langle 110\rangle$ crystal axes.[50] In the excited triplet state, two electrons with parallel spins are localized on the bonding and antibonding orbitals. The probabilities R^+, R^0, and R^- of the spin-selective transitions from the triplet to the ground singlet state are determined by spin-orbit coupling and depend, in general, on the orientation of the crystal in the magnetic field.[54,62,63] The hf structure of the Si-SL1 EPR spectrum due to interactions between electrons and ^{29}Si nuclei occupying the two nearest substitution positions are well resolved and shown in Fig. 3 for the samples with $f_{29\mathrm{Si}} = 4.7$ and 99.2%. For distant nuclei, the dipole-dipole part of hf interaction dominates and leads to the increase in the EPR linewidth with the increase of $f_{29\mathrm{Si}}$. This interaction is responsible for the nuclear spin-lattice relaxation and for optical and dynamic nuclear polarization.

The concentration of Si-SL1 centers has been estimated as follows. The total concentration of A-centers in silicon depends on the dose of irradiation and on the production rate ($\alpha \approx 0.1$ cm^{-1}) of A-centers by 1–1.5 MeV electron irradiation.[57] With the dose of $\Phi \approx 10^{18}$ cm^{-2}, the concentration of A-centers becomes $N(\mathrm{A}) = \alpha\Phi \approx 10^{17}$ cm^{-3}. What fraction of the A-centers is converted to SL1 centers under illumination cannot be determined directly from the EPR spectra because the line intensities depend both on the concentration and spin polarization. Therefore, the concentration of SL1 was estimated by comparing the nuclear polarization times in the phosphorus-doped samples with the known phosphorus concentration $N(\mathrm{P})$.

Under laser photoexcitation, the nuclear polarization time T_{1N}^p in the irradiated samples was ~1 h. A similar value of $T_{1N}^p \approx 1.2$ h was observed in n-Si containing $N(\mathrm{P}) \approx 5 \times 10^{16}$ cm^{-3} paramagnetic phosphorus atoms.[35] Therefore, under high-intensity illumination the concentration of the Si-SL1 centers is comparable with the total concentration of A-centers. It was found that amplitudes of Si-SL1 lines (A–D in Fig. 1) are approximately ten times higher than EPR lines of phosphorus atoms ($N(\mathrm{P}) \approx 5 \times 10^{16}$ cm^{-3}) in the sample measured at 12 K. Taking into account the equilibrium electron polarization of phosphorus $P_{e0} \approx 2\%$ and the number of resonance lines and their linewidths, the steady-state electron spin polarization between $|\pm 1\rangle$ and $|0\rangle$ states of SL1 centers was estimated to be about 70–80%.

B. Optical nuclear polarization

Because DNP experiments with EPR spectroscopy are performed together with the band-gap illumination creating the triplet centers in crystals, let us first reveal the effect of illumination on nuclear spin polarization, i.e., ONP. It was shown that the doping of silicon crystals with different impurities forming deep-energy levels in the gap led to higher ONP degrees.[64] The ONP is induced by the dipole-dipole interaction between localized electrons and distant lattice nuclei in contrast to the DNP that is driven by the contact isotropic hf interactions. The dipole-dipole part (H_{dd}) of hf interaction $H_{\mathrm{hf}} = \boldsymbol{SAI}$ in Eq. (4) between electrons and distant nuclei contains the spin operators ($S_\pm I_\mp$) and ($S_\pm I_\pm$), corresponding to flip-flop ($\Delta m_S = \pm 1$, $\Delta m_I = \mp 1$) and

flip-flip ($\Delta m_S = \pm 1$, $\Delta m_I = \pm 1$) transitions, respectively, and the ($S_z\ I\pm$) term describing only the nuclear spin flip without electron spin transition ($\Delta m_S = 0$, $\Delta m_I = \pm 1$). Probabilities w_1, w_2, and w_3 of flip-flop, flip-flip, and nuclear spin flip transitions, respectively, are given by[43,64]

$$w_1 = \frac{1}{20}\frac{g^2\beta^2 g_N^2\beta_N^2}{r^6}\frac{\tau_c}{1+(\omega_S-\omega_I)^2\tau_c^2}, \quad (5)$$

$$w_1 = \frac{6}{20}\frac{g^2\beta^2 g_N^2\beta_N^2}{r^6}\frac{\tau_c}{1+(\omega_S+\omega_I)^2\tau_c^2}, \quad (6)$$

$$w_3 = \frac{3}{20}\frac{g^2\beta^2 g_N^2\beta_N^2}{r^6}\frac{\tau_c}{1+\omega_I^2\tau_c^2}, \quad (7)$$

where ω_S and ω_I are the electron and nuclear Zeeman frequencies in magnetic field B, respectively, τ_c is the correlation time of the fluctuating electron-nuclear hf interaction. The correlation time for photoexcited triplet centers is determined by random changes of electron spin projections caused by the spin-lattice relaxation with the rate $1/T_{1S}$ and by the recombination rate of triplet centers $1/\tau_T$, where τ_T is their lifetime,

$$\frac{1}{\tau_c} = \frac{1}{T_{1S}} + \frac{1}{\tau_T}. \quad (8)$$

The inversions of some EPR lines of the photoexcited triplet states [see the lines A, B, C, and D in Fig. 1(a)] show that the electron spin-lattice relaxation time is longer than the lifetime, $T_{1S} \gg \tau_T$. For Si-SL1 centers, the lifetime $\tau_T \approx 10^{-3}$ s and spin-lattice relaxation time $T_{1S} > 0.1$ s at $T < 12$ K were reported.[63] The probabilities of the transitions, Eqs. (5)–(7), depend on the magnetic field B and on the correlation time τ_c. Flip-flop (w_1) and flip-flip (w_2) transitions are important only in the weak magnetic fields $B \leqslant (\gamma_S\tau_c)^{-1}$, while the nuclear relaxation probability w_3 is significant in the larger magnetic fields up to $B \approx (\gamma_I\tau_c)^{-1}$. These transitions are responsible for the ONP carried out in weak magnetic fields without microwave saturation of EPR lines.[64,65]

In general, the deviation of nuclear polarization degree P_N from its equilibrium value P_{N0} is given by[64,65]

$$P_N - P_{N0} = -wf_n(P_e - P_{e0}), \quad (9)$$

where

$$w = \frac{w_2 - w_1}{w_1 + 2w_3 + w_2}. \quad (10)$$

Here $f_n \leqslant 1$ is a factor describing the decrease of the nuclear polarization degree due to relaxation caused by extraneous paramagnetic centers and is given by $f_n = 1/(1+f)$, where f is the well-established leakage factor discussed in detail in Ref. 44. The electron polarization of the photoexcited triplet centers P_{eT} is determined as

$$P_{eT} = \frac{N^+ - N^-}{N^+ + N^0 + N^-}, \quad (11)$$

where N^+, N^0, and N^- are the populations of the $|+1\rangle$, $|0\rangle$ and $|-1\rangle$ states, respectively. At $B \gg B_{ac}$, P_{eT} is zero because of the equal populations of the $|+1\rangle$ and $|-1\rangle$ states. At lower magnetic fields, $B \sim B_{ac}$, electron polarization $P_{eT} \neq 0$ is opposite to equilibrium Boltzmann polarization because of the mixing of states with different spin projections.[65] The maximum values of P_{eT} and, consequently, P_N, are achieved at $B = B_{ac}$.

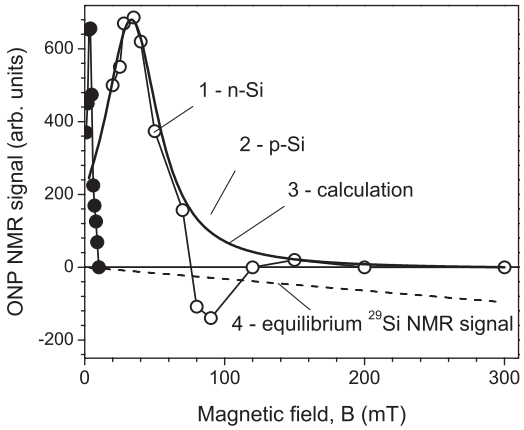

FIG. 4. Optically enhanced ^{29}Si NMR signal intensity vs magnetic field B observed in the 1-MeV electron irradiated n-Si ($N(\mathrm{P}) \approx 5 \times 10^{16}$ cm^{-3}) (o: curve 1) and the high-resistance (~1000 Ω. cm) p-type Si (•: curve 2) with the natural abundance (4.7%) of the ^{29}Si isotope after 15 min of illumination by the 100-mW halogen lamp at $T = 8$ K and $B \,||\, \langle 111\rangle$. Curve 3 is the calculated dependence of P_N on B normalized by the maximal value at $B = B_{ac}$. Curve 4 shows the dependence of the equilibrium ^{29}Si NMR signal on B. Hereafter, the positive and negative signs of NMR signals correspond to DNP in opposite and the same directions with respect to equilibrium nuclear polarization, respectively.

Figure 4 shows the dependences of the ^{29}Si NMR signal intensity on the magnetic field, observed after band-gap illumination of the electron irradiated phosphorus-doped (curve 1) and high-resistance p-type (curve 2) silicon samples. Curve 3 shows the calculated dependence of P_N on the magnetic field using the Eqs. (5)–(7) and (8)–(11) and taking into account the mixing of the triplet spin states for different orientations of Si-SL1 centers in the silicon lattice in the manner similar to calculations performed in Ref. 65. For comparison, the intensity of the equilibrium NMR signal estimated from the equilibrium signal detected at room temperature and $B = 7$ T are shown by a dashed line (curve 4, Fig. 4). The negative NMR signals, which are the same sign as that for equilibrium ^{29}Si NMR signals, observed in n-type Si (see curve 2 in Fig. 4) are explained by ONP due to dipole-dipole interaction between electrons localized at phosphorus atoms and ^{29}Si nuclei. In p-type Si, only the positive NMR signals corresponding to ONP of ^{29}Si mediated by Si-SL1 centers are observed after illumination. Figure 4 shows that ONP is effective only in weak magnetic fields. The enhancement E of ONP-NMR signals extrapolated to the infinite time of illumination at $B = 35$ mT and $T = 8$ K is $E^{ss} \approx 520$. However, the effect of ONP in the following DNP experiments is negligible since they will be performed at a higher magnetic, $B \sim 300$–360 mT.

C. Dynamic nuclear polarization

Figure 5 shows the ^{29}Si NMR signals observed after a 10-min saturation at the magnetic fields corresponding to the maxima of the Si-SL1 EPR line. Here, significantly stronger NMR signals exceeding 10^3 to 10^4 times the equilibrium NMR

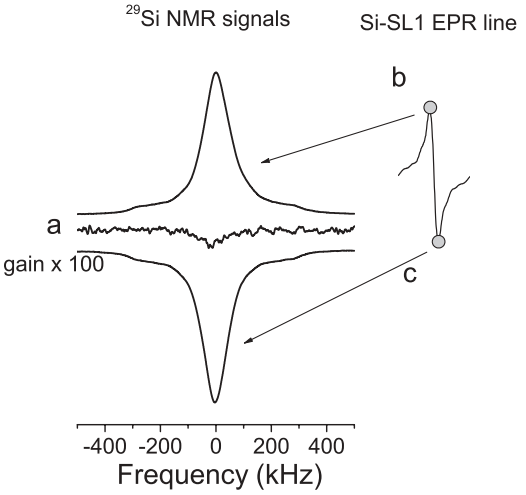

FIG. 5. The equilibrium ^{29}Si NMR signal (line labeled a) and the ^{29}Si NMR signal in the naturally abounded n-type Cz-grown electron irradiated silicon after 10 min saturation at $T = 12$ K of the Si-SL1 EPR line at the positions b and c corresponding to the maxima of the first-derivative EPR line shape. The NMR measurements were performed at 300 K and $B = 7$ T.

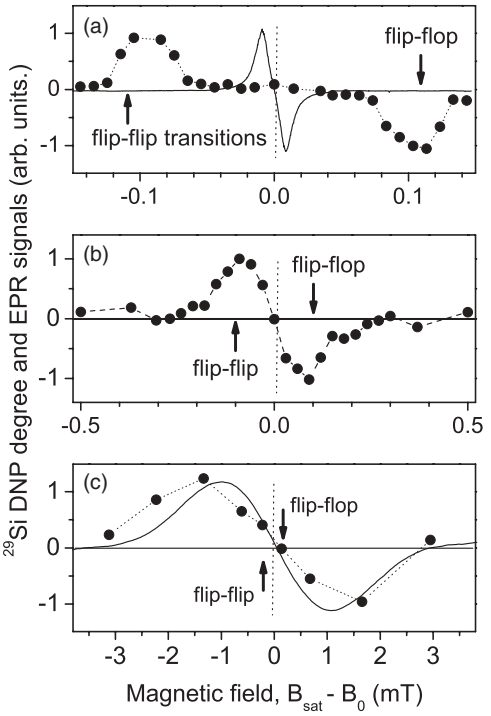

FIG. 6. Dependences of the ^{29}Si polarization (NMR signal intensities after DNP) on the magnetic fields B_{sat} employed for the DNP in the X-band EPR spectrometer for n-Si samples containing 0.59% (a), 4.7% (b), and 99.2% (c) ^{29}Si isotopes. Solid curves show the first derivative of the Si-SL1 EPR lines at $B_0 = 357.5$ mT. Both the NMR and EPR signal intensities are normalized by taking their maximum values as unity. The ^{29}Si NMR signals were acquired at $T = 300$ K and $B = 7$ T after microwave saturation for 10 min with $B_{sat} \parallel \langle 110 \rangle$, $T_{sat} = 20$ K, and 100-W halogen lamp illumination. Arrows show the positions of flip-flip and flip-flop transitions at $\Delta B_{\pm}$ (see text for details). The dotted lines are guide to eyes. The NMR signals corresponding to equilibrium polarization at $B = 7$ T and $T = 300$ K are very small (in units of vertical axes): -5.5×10^{-4}, -5×10^{-4}, and -1.8×10^{-2} for samples (a), (b), and (c), respectively.

signals were observed. Similar DNP enhancements of the NMR signal were observed for saturation of other Si-SL1 EPR lines, indicating that each EPR transition involves a strong nonequilibrium electron polarization. In contrast to ONP, where nuclear polarization is due to the difference in the relaxation with the probabilities given by Eqs. (5)–(7), DNP is driven by the flip-flop and flip-flip transitions between the electron and ^{29}Si nuclear spins that are induced by the resonance microwave field, with the frequency tuned specifically to each transition. To reveal the DNP mechanism, the orientation of ^{29}Si was obtained by saturation of the EPR transitions of Si-SL1 centers at different magnetic fields, B_{sat}, using the EPR spectrometer, and the resulting polarization of ^{29}Si was determined by NMR by comparing the first-derivative EPR line shape. Figure 6 shows that the DNP of ^{29}Si nuclei is a result of solid-effect[43–45] due to saturation of the forbidden flip-flop and flip-flip transitions corresponding to the electron and distant ^{29}Si nuclear spin flips in the opposite and in the same directions, respectively. The shift, $\Delta B_{\pm}$, of the forbidden flip-flop and flip-flip transitions from the center of the EPR line at $B_0 \cong 357.5$ mT is equal to $\Delta B_{\pm} = B - B_0 = \pm B_0(\gamma_n/\gamma_e) = \pm 0.11$ mT for ^{29}Si nuclei.

As can be seen from Fig. 6(a), the value of ΔB exceeds the peak-to-peak linewidth (PPLW) of the Si-SL1 EPR signal in the 0.59% ^{29}Si sample. Two peaks of ^{29}Si DNP at $\Delta B_{\pm} \approx \pm 0.11$ mT corresponding to the flip-flop and flip-flip transitions lead to the opposite signs of nuclear polarization. This is a good example of the so-called resolved solid-effect.[43–45] As can be seen from Fig. 6(a), the regions of magnetic fields where DNP arises under microwave saturation of the flip-flip and flip-flop transitions exceed the PPLW of the EPR line. Furthermore, these ranges are shifted slightly from the exact positions of the flip-flip and flip-flop transitions marked by arrows toward the central line. This can be explained by a small contribution of dipole-dipole interactions between electron and distant nuclear spins. In the 4.7% ^{29}Si sample [Fig. 6(b)], the PPLW is comparable with the splitting between the forbidden flip-flop and flip-flip transitions, and DNP is therefore due to partly resolved solid-effects. The satellites observed near the EPR line at ± 0.35 and ± 0.1 mT are caused by hf interaction with the ^{29}Si nuclei occupying the places in the second and third lattice shells of the A-center, respectively. The hf interaction with more distant nuclei is weaker, gives the contribution to the EPR linewidth, and is responsible for the DNP expansion across the sample by the nuclear spin diffusion process. The EPR lines of the Si-SL1 spectrum in the 99% ^{29}Si sample [see Fig. 6(c)] are broadened by dipole-dipole interaction with the ^{29}Si lattice nuclei. The PPLW exceeds the value $2\Delta B_{\pm} \approx \pm 0.22$ mT, and the shape of P_N dependence on B_{sat} resembles the shape of the first derivative of the EPR line. This indicates that DNP is a result of differential solid-effect.[44] Here, the microwave field saturates the forbidden flip-flop and flip-flip transitions of different spin packets at the same time to result in significantly fewer polarization degrees of ^{29}Si.

TABLE I. Summary of DNP experiments performed at 3.1 to 3.2 K. Types of DNP are cauterized as resolved solid effect (RSE), partially resolved solid effect (PRSE), and differential solid effect (DSE). The nuclear spin polarization time T_{1N}^{p} and steady-state ^{29}Si DNP degree P_N^{ss} are given.

			P_N^{ss} %	
Sample	DNP	T_{1N}^{p} min	$B \,||\, \langle 110\rangle$	$B \,||\, \langle 111\rangle$
0.59% ^{29}Si	RSE	75	6.41	–
4.7% ^{29}Si	PRSE	72	6.37	(9–11)[a] (13–16)[b]
99.2% ^{29}Si	DSE	59	0.17	0.97

[a]An estimated steady-state DNP degree for $B \,||\, \langle 111\rangle$ when simultaneous saturation of two completely overlapping Si-SL1 lines is realized experimentally.
[b]An estimated steady-state DNP degree for $B \,||\, \langle 111\rangle$ when simultaneous saturation of three completely overlapping Si-SL1 lines is realized experimentally.

The DNP degree P_N increases exponentially in time t and approaches its steady-state value P_N^{ss}. It was found that the nuclear polarization rate $1/T_{1N}^{p}$, determined by exponential fit of the experimental dependences of P_N on t, increases with the light intensity that produces higher concentrations of the triplet centers. The intensity of Si-SL1 EPR lines and P_N are in accordance with this picture for the temperature range 4–20 K but decreases at higher temperatures in accordance with our earlier investigations.[40] Such a decrease of P_N at $T > 20$ K is explained by the decrease in electron spin-lattice relaxation, which, in turn, decreases the electron spin polarization degree between magnetic sublevels of Si-SL1 centers.[40,61]

To achieve the higher DNP degree in shorter time, we used the laser excitation at the light power up to 700 mW. To prevent the heating of samples by high light intensity, the experiments were performed at temperatures 3.1–3.2 K that were realized by the direct contact with the pumped liquid helium. The results are summarized in Table I. Here, the electron spin polarization between the magnetic sublevels of the triplet center was estimated (see Sec. III A) as $P_e \sim 70$–80%. The DNP degree obtained by saturation of the flip-flop or flip-flip transitions of only one of the 12 available EPR lines of Si-SL1 already led to a very impressive ~6.4%, which is large enough to implement the efficient algorithmic cooling protocol[28] to increase the polarization further for initialization. This ~6.4%, however, is still limited by the extraneous nuclear relaxation caused by paramagnetic centers that do not participate in the DNP process because the A-centers are oriented in the Si lattice along six equivalent $\langle 110\rangle$ axes. Due to this symmetry, Si-SL1 centers yield 12 EPR lines. Therefore, DNP with $B \,||\, \langle 110\rangle$ uses only one of 12 EPR transitions, and the remaining 11 transitions can be considered as paramagnetic centers, leading to suppression of the DNP degree with the factor $f_n = 1/12 \approx 0.083$. The six-time increase of the DNP degree is expected for the orientation $B \,||\, \langle 111\rangle$ by saturating simultaneously all the Si-SL1 EPR lines that group together around the same magnetic field [see Fig. 1(b)]. Figure 7 shows results of a proof-of-concept experiment to demonstrate nearly a sixfold increase in DNP degrees, 0.17 to 0.97 as listed in Table I, for $B \,||\, \langle 111\rangle$, with respect to that in $B \,||\, \langle 110\rangle$ in the 99.2% isotopically enriched ^{29}Si sample. The Si-SL1 EPR lines in this sample are broadened by hf interaction overlap very well [Fig. 3(c)], i.e., and simultaneous excitations of different lines are possible with an expense of overall fewer DNP degrees due to the differential solid effect. However, Si-SL1 EPR lines in the ^{29}Si <4.7% samples are very narrow [Fig. 1(b)], and it is possible to adjust the angle and magnetic field since only two or three Si-SL1 EPR lines overlap. In such experiments approximately a two- or three-time increase of DNP NMR signals was detected. Unfortunately, it is difficult to reproduce exactly the same sample position (orientation) in the EPR spectrometer after the measurement of the NMR signal to determine the steady-state DNP degree. The estimated steady-state DNP degrees P_N^{ss} for naturally abounded irradiated Si sample are listed in the Table I (column 5). In the future, if all of the 12 transitions could be saturated by applying 12 microwave resonance frequencies simultaneously, the nuclear polarization degree would be $6.4\% \times 12 = 76.8\%$, which is approximately equal to the estimated electron spin polarization. Therefore, the electron polarization of the SL1, in principle, is being transferred to the nearest-neighbor ^{29}Si nuclear system very efficiently without much loss.

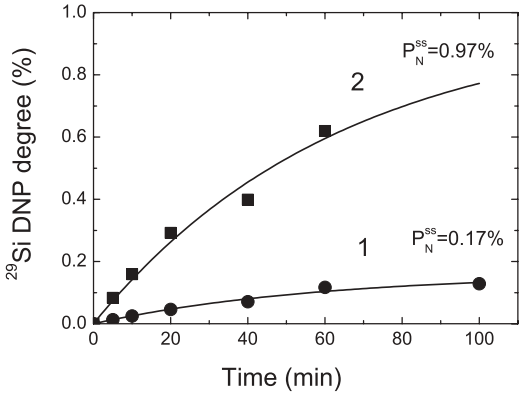

FIG. 7. The DNP degree vs saturation time for 99.2% ^{29}Si sample with saturation of only one EPR line with $B \,||\, \langle 110\rangle$ (curve 1) and six lines with $B \,||\, \langle 111\rangle$ (curve 2) measured at $T = 12$ K and with the laser light power 300 mW. Solid curves are the exponential fits.

In addition, EPR lines corresponding to the forbidden $\Delta m_S = \pm 2$ transition were observed in all samples at $B \approx 160$ mT. These lines have a weak angular dependence, and all lines overlap well regardless of the ^{29}Si abundance. The total electron spin polarization at $B \approx 160$ mT is also not equal to Boltzmann polarization because of the mixing of $|+1\rangle$, $|0\rangle$, and $|-1\rangle$ states; therefore, the DNP can be realized by saturation of the flip-flop and flip-flip electron-nuclear transitions. However, DNP obtained by saturation of the $\Delta m_S = \pm 2$ line of natural silicon reached $P_N^{ss} \approx 0.56\%$ only with the nuclear polarization time $T_{1N}^{p} \approx 61$ min.

D. DNP by saturation of the Si-SL1 hf lines

It was found that DNP could be realized by microwave excitation of electron-nuclear transitions not only within the central Si-SL1 EPR lines but also by excitation of satellites arising from hf interactions between the SL1 electron and the nearest ^{29}Si nuclear spins. Figure 8 shows the dependence of

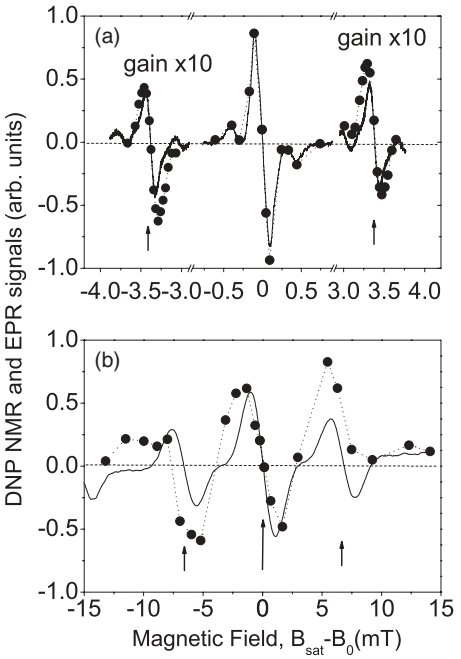

FIG. 8. The dependences of the ^{29}Si DNP NMR signal amplitude on the magnetic field $B_{\rm sat}$ (•) for $B \,||\, \langle 110\rangle$ and $B_0 = 359.7$ mT and the first derivative of the Si-SL1 EPR lines (solid curves) corresponding to the transitions between $|+1\rangle$ and $|0\rangle$ states for the 4.7% (a) and 99.2% ^{29}Si (b) samples. The EPR lines marked by arrows are satellites due to the hf interaction between the SL1 electron and the nearest-neighbor ^{29}Si nuclear spins.

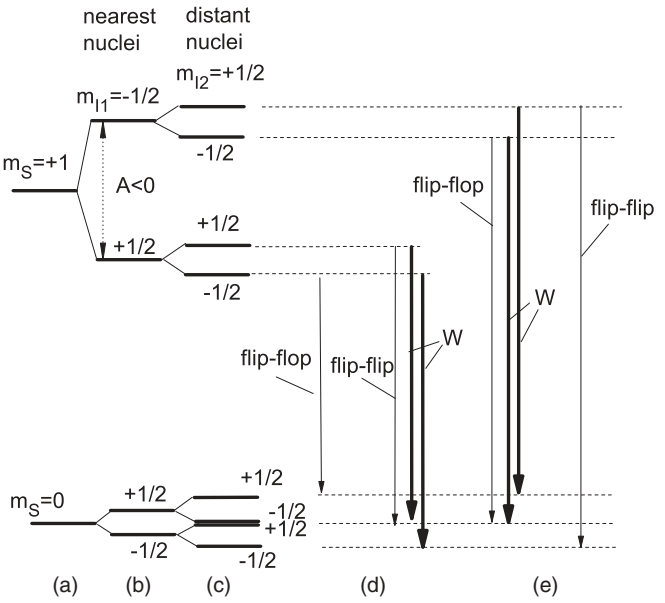

FIG. 9. Energy level diagram (not in scale) showing the electron Zeeman splitting between $|+1\rangle$ and $|0\rangle$ spin states of Si-SL1 center (a), hf splitting due to interaction between electron and nearest nuclear spin (b), nuclear Zeeman splitting by distant ^{29}Si nuclei (c), and possible transitions between energy levels induced by microwave field (d) and (e).

the DNP NMR signal amplitude on the magnetic field for the high-field line D [see Fig. 1(a)] in comparison with the first-derivative EPR lines for 4.7 and 99.2% ^{29}Si samples. The lines marked by arrows are the hf structure lines. While the DNP degree follows approximately the first-derivative shape of the central EPR line, there is a clear asymmetry in the dependence of the DNP degree on the magnetic; the negative NMR signals corresponding to saturation of the flip-flop transitions of the low-field hf-line are stronger than the positive signals caused by saturation of the flip-flip transitions. For the high-field hf line, the ratio between positive and negative signals is opposite. Similar asymmetries of DNP were observed for hf lines of all EPR transitions of Si-SL1 centers.

Asymmetry of DNP caused by saturation of hf lines can be explained by considering the simple energy level (Fig. 9) for microwave-induced transitions of the coupled SL1 electron and distant ^{29}Si nuclear spin system. Let us consider an EPR transition between $m_S = +1$ and $m_S = 0$ states corresponding to the EPR line at 360 mT for $B \,||\, \langle 110\rangle$ [see Fig. 1(a) and Fig. 7]. The electron Zeeman splitting between these states is shown in Fig. 9(a). The hf interaction with the nearest ^{29}Si nuclei splits $m_S = +1$ state but not the $m_S = 0$ state. Taking into account negative sign of the hf interaction constant $A = -184$ MHz for Si-SL1 center for $B \,||\, \langle 110\rangle$,[50] the energy level corresponding to $m_{I1} = -1/2$ will be higher than the level corresponding to $m_{I1} = +1/2$ for $m_S = +1$ state [see Fig. 9(b)]. The energy levels for a system, including the dipolar interactions with the second-nearest neighbor ^{29}Si nuclei, are shown in Fig. 9(c). Neglecting the weak hf interactions between these nuclei and electron spins, the spitting of $m_{I2} = \pm 1/2$ is equal to the nuclear Zeeman frequency. The flip-flop and flip-flip transitions leading to DNP of the second-nearest-neighbor ^{29}Si are shown by arrows in Figs. 9(d) and 9(e). Here, the flip-flip transitions between electron and distant nuclear spins $|+1, +1/2, +1/2\rangle \leftrightarrow |0, +1/2, -1/2\rangle$ [Fig. 9(d)] correspond to the high-field hf line [see Fig. 8(a)], and additional flip-flip transitions exist as for the nearest-neighbor nuclei $|+1, +1/2, +1/2\rangle \leftrightarrow |0, -1/2, +1/2\rangle$ and $|+1, +1/2, -1/2\rangle \leftrightarrow |0, -1/2, -1/2\rangle$. For the low-field hf line, the additional flip-flop transitions correspond to $|+1, -1/2, +1/2\rangle \leftrightarrow |0, +1/2, +1/2\rangle$ and $|+1, -1/2, -1/2\rangle \leftrightarrow |0, +1/2, -1/2\rangle$. These additional transitions (W) lead to the spin polarization of nearest-neighbor nuclei in the manner more negative for the low-field hf line and more positive for the high-field hf line, as seen in Fig. 8.

E. Impact of the present study on silicon quantum information processing

Because the lifetime of the triplet states (SL1) of O-V centers is only a few milliseconds,[27] it is not practical to employ the spin-triplet state of SL1 as a qubit or qutrit in which three levels are used for quantum information processing. However, taking advantage of this short lifetime, SL1 can be regarded as an on-demand qubit manipulator by controlling the timing of light illumination to form SL1. Otherwise, it stays in the singlet ground state of an O-V center, which is nonparamagnetic, i.e., it is immune from decohering nearby working qubits. Consequently, there are two ways of implementing SL1 centers for silicon-based quantum information processing: (i) as a quantum information input source and

readout node of the nearby ^{29}Si nuclear spin qubits, as already shown in Ref. 27, and (ii) as a ^{29}Si nuclear spin polarizer in order to reduce the magnetic fluctuation in silicon to protect other qubits from decoherence. The present study sheds light on the latter issue (ii). Currently, phosphorus[12,13,21–23] and bismuth[66] donors and gate-defined quantum dots[14] are the most experimentally advanced qubits in silicon. For implementation of such qubits, isotopically enriched ^{28}Si or ^{30}Si single crystals that are depleted of the background ^{29}Si nuclear spins are preferred since the magnetic field fluctuation arising from flip-flops among ^{29}Si nuclear spins serves as a source of decoherence. However, one can employ naturally available silicon with 4.7% ^{29}Si if the majority of background ^{29}Si nuclear spins can be polarized to suppress the flip-flops. For such purposes, Si-SL1 centers are ideal since, as shown in the present study, it is feasible in the future to achieve up to ∼77% of the ^{29}Si polarization spanning the entire silicon sample by saturating the spin-triplet levels of SL1. Moreover, after achieving the needed polarization, termination of the light illumination causes Si-SL1 decays to O-V singlet states in a few milliseconds to become ineffective decoherence sources for working qubits. An additional advantage of the present scheme is that it can be applied in both n-type and p-type silicon. The process to introduce O-V centers throughout the sample is rather straightforward. One can take commercially available Czochralski silicon, which typically contains 10^{18} cm^{-3} of oxygen, and gamma irradiate it with a simple cobalt source or the like.

IV. CONCLUSIONS

The photoexcited spin $S = 1$ states (Si-SL1 centers) of the oxygen + vacancy complexes (A-centers) have been employed for DNP of ^{29}Si nuclei. The steady-state electron spin polarization between the triplet spin states $|\pm 1\rangle$ and $|0\rangle$ was found to be 70–80%, and such high electron polarization was transferred successfully to the lattice ^{29}Si nuclei by solid-effect using the microwave saturation of the electron-nuclear flip-flop and flip-flip transitions. The ^{29}Si DNP degree ∼6.4% was achieved after 2 to 3 h of saturation of only one of 12 Si-SL1 EPR lines. The remaining 11 EPR transitions of Si-SL1 centers lead to extraneous nuclear relaxation, limiting DNP degree with factor f_n about 0.083. It was shown that the efficiency of DNP can be increased by saturation of several EPR lines. In 99.2% ^{29}Si isotope-enriched sample the saturation of the EPR lines of Si-SL1 centers with magnetic field $B \,||\, \langle 111 \rangle$ leads to the six times higher DNP degree when the EPR lines overlap completely. It was demonstrated in silicon with ^{29}Si isotope abundance $\leqslant$4.7% that the simultaneous saturation of two (or three) EPR lines increases the DNP degree two (or three) times.

The present systematic study has shown that optical polarization of the ^{29}Si nuclei is effective only in weak magnetic fields $B < 100$ mT, and contribution of this optical orientation is negligibly small in the DNP process. The transformation of the DNP mechanisms from the resolved to differential solid-effect was found with the increasing abundance of ^{29}Si. DNP was observed not only under saturation of the electron-nuclear flip-flop and flip-flip transitions but also by saturation the hf satellite EPR transitions arising from the interactions with the nearest ^{29}Si nuclei. Asymmetries in the DNP line shape were observed due to additional flip-flop and flip-flip transitions between SL1 electrons and nearest-neighbor ^{29}Si nuclear spins.

ACKNOWLEDGMENTS

The authors thank the Central Service Facilities for Research in Keio University for the provision of the well-developed experimentation environment. This work was supported in part by Grant-in-Aid for Scientific Research No. 22241024 by MEXT, in part, by Special Coordination Funds for Promoting Science and Technology and, in part, by FIRST.

*Corresponding author: kitoh@appi.keio.ac.jp

[1] K. M. Itoh, J. Kato, F. Uemura, A. K. Kaliteyevskii, O. N. Godisov, G. G. Devyatych, A. D. Bulanov, A. V. Gusev, I. D. Kovalev, P. G. Sennikov, H.-J. Pohl, N. V. Abrosimov, and H. Riemann, Jpn. J. Appl. Phys. Part 1 **42**, 6248 (2003).

[2] K. Takyu, K. M. Itoh, K. Oka, N. Saito, and V. I. Ozhogin, Jpn. J. Appl. Phys. **38**, L1493 (1999).

[3] T. Kojima, R. Nebashi, K. M. Itoh, and Y. Shiraki, Appl. Phys. Lett. **83**, 2318 (2003).

[4] Y. Shimizu, M. Uematsu, and K. M. Itoh, Phys. Rev. Lett. **98**, 095901 (2007).

[5] J. Sailer, V. Lang, G. Abstreiter, G. Tsuchiya, K. M. Itoh, J. W. Ager, III, E. E. Haller, D. Kupidura, D. Harbusch, S. Ludwig, and D. Bougeard, Phys. Status Solidi RRL **3**, 61 (2009).

[6] A. Wild, J. Kierig, J. Sailer, J. W. Ager, III, E. E. Haller, G. Abstreiter, S. Ludwig, and D. Bougeard, Appl. Phys. Lett. **100**, 143110 (2012).

[7] B. E. Kane, Nature (London) **393**, 133 (1998).

[8] T. D. Ladd, J. R. Goldman, F. Yamaguchi, Y. Yamamoto, E. Abe, and K. M. Itoh, Phys. Rev. Lett. **89**, 017901 (2002).

[9] K. M. Itoh, Solid State Commun. **135**, 747 (2005).

[10] J. J. L. Morton, D. R. McCamey, M. A. Eriksson, and S. A. Lyon, Nature (London) **479**, 345 (2011).

[11] H. Wu, R. E. George, J. H. Wesenberg, K. Mølmer, D. I. Schuster, R. J. Schoelkopf, K. M. Itoh, A. Ardavan, J. J. L. Morton, and G. A. D. Briggs, Phys. Rev. Lett. **105**, 140503 (2010).

[12] A. Morello, J. J. Pla, F. A. Zwanenburg, K. W. Chan, K. Y. Tan, H. Huebl, M. Möttönen, C. D. Nugroho, C. Yang, J. A. van Donkelaar, A. D. C. Alves, D. N. Jamieson, C. C. Escott, L. C. L. Hollenberg, R. G. Clark, and A. S. Dzurak, Nature (London) **467**, 687 (2010).

[13] M. Fuechsle, J. A. Miwa, S. Mahapatra, H. Ryu, S. Lee, O. Warschkow, L. C. L. Hollenberg, G. Kimeck, and M. Y. Simmons, Nat. Nanotechnol. **7**, 242 (2012).

[14] C. B. Simmons, J. R. Prance, B. J. Van Bael, T. S. Koh, Z. Shi, D. E. Savage, M. G. Lagally, R. Joynt, M. Friesen, S. N. Coppersmith, and M. A. Eriksson, Phys. Rev. Lett. **106**, 156804 (2011).

[15]S. Simmons, R. M. Brown, H. Riemann, N. V. Abrosimov, P. Becker, H.-J. Pohl, M. L. W. Thewalt, K. M. Itoh, and J. J. L. Morton, Nature (London) **470**, 69 (2011).
[16]A. Yang, M. Steger, D. Karaiskaj, M. L. W. Thewalt, M. Cardona, K. M. Itoh, H. Riemann, N. V. Abrosimov, M. F. Churbanov, A. V. Gusev, A. D. Bulanov, A. K. Kaliteevskii, O. N. Godisov, P. Becker, H.-J. Pohl, J. W. Ager, III, and E. E. Haller, Phys. Rev. Lett. **97**, 227401 (2006).
[17]A. Yang, M. Steger, T. Sekiguchi, M. L. W. Thewalt, T. D. Ladd, K. M. Itoh, H. Riemann, N. V. Abrosimov, P. Becker, and H.-J. Pohl, Phys. Rev. Lett. **102**, 257401 (2009).
[18]M. Steger, T. Sekiguchi, A. Yang, K. Saeedi, M. E. Hayden, M. L. W. Thewalt, K. M. Itoh, H. Riemann, N. V. Abrosimov, P. Becker, and H.-J. Pohl, J. Appl. Phys. **109**, 102411 (2011).
[19]M. Steger, K. Saeedi, M. L. W. Thewalt, J. J. L. Morton, H. Riemann, N. V. Abrosimov, P. Becker, and H.-J. Pohl, Science **336**, 1280 (2012).
[20]A. M. Tyryshkin, S. A. Lyon, A. V. Astashkin, and A. M. Raitsimring, Phys. Rev. B **68**, 193207 (2003).
[21]E. Abe, K. M. Itoh, J. Isoya, and S. Yamasaki, Phys. Rev. B **70**, 033204 (2004).
[22]E. Abe, A. M. Tyryshkin, S. Tojo, J. J. L. Morton, W. M. Witzel, A. Fujimoto, J. W. Ager, E. E. Haller, J. Isoya, S. A. Lyon, M. L. W. Thewalt, and K. M. Itoh, Phys. Rev. B **82**, 121201(R) (2010).
[23]A. M. Tyryshkin, S. Tojo, J. J. L. Morton, H. Riemann, N. V. Abrosimov, P. Becker, H.-J. Pohl, T. Schenkel, M. L. W. Thewalt, K. M. Itoh, and S. A. Lyon, Nat. Mater. **11**, 143 (2012).
[24]A. S. Verhulst, D. Maryenko, Y. Yamamoto, and K. M. Itoh, Phys. Rev. B **68**, 054105 (2003).
[25]T. D. Ladd, D. Maryenko, Y. Yamamoto, E. Abe, and K. M. Itoh, Phys. Rev. B **71**, 014401 (2005).
[26]A. E. Dementyev, D. Li, K. MacLean, and S. E. Barrett, Phys. Rev. B **68**, 153302 (2003).
[27]W. Akhtar, V. Filidou, T. Sekiguchi, E. Kawakami, T. Itahashi, L. Vlasenko, J. J. L. Morton, and K. M. Itoh, Phys. Rev. Lett. **108**, 097601 (2012).
[28]L. J. Schulman and U. V. Vazirani, in *Proceedings of the 31st ACM Symposium on Theory of Computing* (ACM Press, New York, 1999), p. 322.
[29]A. Abragam, J. Combrisson, and I. Solomon, C. R. Acad. Sci. **246**, 1035 (1958).
[30]A. Abragam, J. Combrisson, and I. Solomon, C. R. Acad. Sci. **247**, 2337 (1958).
[31]G. Lampel, Phys. Rev. Lett. **20**, 491 (1968).
[32]N. T. Bagraev and L. S. Vlasenko, Fiz. Tverd. Tela (Leningrad) **24**, 3470 (1982) [Sov. Phys. Solid State **24**, 1974 (1982)].
[33]A. S. Verhulst, I. G. Rau, Y. Yamamoto, and K. M. Itoh, Phys. Rev. B **71**, 235206 (2005).
[34]H. Hayashi, W. Ko, T. Itahashi, A. Sagara, K. M. Itoh, L. S. Vlasenko, and M. P. Vlasenko, Phys. Status Solidi C **3**, 4388 (2006).
[35]H. Hayashi, T. Itahashi, K. M. Itoh, L. S. Vlasenko, and M. P. Vlasenko, Phys. Rev. B **80**, 045201 (2009).
[36]G. Feher and E. A. Gere, Phys. Rev. **114**, 1245 (1959).
[37]M. R. Rahman, T. Itahashi, M. P. Vlasenko, L. S. Vlasenko, E. E. Haller, and K. M. Itoh, Jpn. J. Appl. Phys. **49**, 103001 (2010).
[38]A. E. Dementyev, D. G. Cory, and C. Ramanathan, Phys. Rev. Lett. **100**, 127601 (2008).
[39]A. E. Dementyev, D. G. Cory, and C. Ramanathan, J. Chem. Phys. **134**, 154511 (2011).
[40]L. S. Vlasenko, M. P. Vlasenko, D. S. Poloskin, R. Laiho, H. Hayashi, T. Itahashi, A. Sagara, and K. M. Itoh, Phys. Status Solidi C **3**, 4376 (2006).
[41]T. Itahashi, H. Hayashi, K. M. Itoh, D. S. Poloskin, L. S. Vlasenko, and M. P. Vlasenko, Physica B **404**, 5054 (2009).
[42]A. W. Overhauser, Phys. Rev. **92**, 411 (1953).
[43]A. Abragam, *The Principles of Nuclear Magnetism* (Oxford University Press, Oxford, 1961).
[44]O. S. Leifson and C. D. Jeffries, Phys. Rev. **122**, 1781 (1961).
[45]T. J. Schmugge and C. D. Jeffries, Phys. Rev. **138**, A1785 (1965).
[46]H. Schuch, D. Stehlik, and K. H. Hausser, Z. Naturforsch. A **26**, S.1944 (1971).
[47]H. W. van Kesteren, W. Th. Wenckebach, J. Schmidt, and N. J. Poulis, Chem. Phys. Lett. **89**, 67 (1982).
[48]H. W. van Kesteren, W. Th. Wenckebach, and J. Schmidt, Phys. Rev. Lett. **55**, 1642 (1985).
[49]A. Henstra, P. Dirksen, J. Schmidt, and W. T. Wenckebach, J. Magn. Reson. **77**, 389 (1988).
[50]K. L. Brower, Phys. Rev. B **4**, 1968 (1971).
[51]G. D. Watkins, Phys. Rev. **155**, 802 (1967).
[52]G. D. Watkins, Phys. Rev. B **12**, 4383 (1975).
[53]V. A. Khramtsov, V. N. Lomasov, Ya. Ya. Pilkevich, M. P. Vlasenko, and L. S. Vlasenko, Phys. Status Solidi A **109**, 127 (1988).
[54]L. S. Vlasenko, Yu. V. Martynov, T. Gregorkiewicz, and C. A. J. Ammerlaan, Phys. Rev. B **52**, 1144 (1995).
[55]L. S. Vlasenko, Phys. Solid State **41**, 697 (1999).
[56]M. P. Vlasenko and L. S. Vlasenko, Sov. Phys. Solid State **33**, 1326 (1991).
[57]J. W. Corbett, G. D. Watkins, R. M. Chrenko, and R. S. McDonald, Phys. Rev. **121**, 1015 (1961).
[58]V. Eremin, D. S. Poloskin, E. Verbitskaya, M. P. Vlasenko, L. S. Vlasenko, R. Laiho, and T. O. Niinikoski, J. Appl. Phys. **93**, 9659 (2003).
[59]R. Laiho, L. S. Vlasenko, M. P. Vlasenko, V. A. Kozlov, and V. V. Kozlovski, Appl. Phys. Lett. **74**, 3948 (1999).
[60]W. Akhtar, T. Sekiguchi, T. Itahashi, V. Filidou, J. J. L. Morton, L. Vlasenko, and K. M. Itoh, Phys. Rev. B **86**, 115206 (2012).
[61]H. Hayashi, K. M. Itoh, and L. S. Vlasenko, Phys. Rev. B **78**, 153201 (2008).
[62]S. P. McGlynn, T. Azumi, and M. Kinoshita, *Molecular Spectroscopy of the Triplet State* (Prentice-Hall, Englewood Cliffs, NJ, 1969).
[63]L. S. Vlasenko, I. M. Zaritskii, A. A. Konchits, and B. D. Shanina, Sov. Phys. Solid State **26**, 66 (1984).
[64]N. T. Bagraev and L. S. Vlasenko, Sov. Phys. JETP **48**, 878 (1978).
[65]L. S. Vlasenko, M. P. Vlasenko, V. N. Lomasov, and V. A. Khramtsov, Sov. Phys. JETP **64**, 612 (1986).
[66]P. A. Mortemousque, T. Sekiguchi, C. Culan, M. P. Vlasenko, R. G. Elliman, L. S. Vlasenko, and K. M. Itoh, Appl. Phys. Lett. **101**, 082409 (2012), and references therein.